RSC Advances

PAPER

View Article Online
View Journal | View Issue

Cite this: *RSC Adv.*, 2023, **13**, 23505

Polyaniline-modified halloysite nanotubes as high-efficiency adsorbents for removing of naproxen in the presence of different heavy metals

Qihui Wang,[a] Minghui Huang,[a] Ying Zhu,[a] Jiexue Wang,[a] Zihang He,[a] Jun Liu,[b] Kang Sun,[a] Zhonghui Li*[a] and Guowei Deng*[a]

Received 1st June 2023
Accepted 31st July 2023

DOI: 10.1039/d3ra03671e

rsc.li/rsc-advances

In this work, novel adsorbent polyaniline-modified halloysite nanotubes (HNT@PA-2) were synthesized successfully by *in situ* polymerization to increase active adsorption sites. With the increase of the amount of aniline, the adsorption capacity of naproxen becomes higher. The optimal ratio of halloysite nanotubes to aniline was 1 : 2. The effects of adsorption conditions such as pH, mass of HNT@PA-2, time and initial concentration of naproxen were systematically researched. The optimum adsorption for naproxen was pH 9, mass 10 mg and contact time 4 h. The adsorption of naproxen conformed to the pseudo-first-order kinetic model, and the maximum adsorption capacity was 242.58 mg g^{-1} at 318 K. In addition, the effects of ionic strength and different heavy metals also were studied. Higher ionic strength of the system could influence the adsorption of naproxen. The effects of Al^{3+}, Pb^{2+}, Zn^{2+} and Co^{2+} ions on the adsorption of naproxen could be ignored, while Cu^{2+} and Fe^{3+} ions inhibited the process. The mechanisms for naproxen adsorbed by the HNT@PA-2 were $\pi-\pi$ interaction, hydrogen bonding and hydrophobic reaction. Therefore, the HNT@PA-2 could be used for the treatment of medical wastewater for removing naproxen.

Introduction

Non-steroidal anti-inflammatory drugs (NSAIDs) are a class of antipyretic, analgesic, and anti-inflammatory drugs that do not contain steroid structures.[1,2] Since aspirin was first synthesized in 1898, more than one hundred types of NSAID have been marketed under thousands of brands over the past one hundred years. Currently, NSAIDs are some of the most widely used drugs in the world. Around 30 million people worldwide use them every day. Naproxen as a typical NSAID is widely used for the reduction of pain and inflammation effectively.[3] As the use of naproxen increases, their amount entering the environment grows rapidly. Naproxen is continuously detected in drinking water, seawater and ground water because it is not easily treated thoroughly by wastewater treatment systems.[4,5] Naproxen residues in the environment not only affect the water quality, but also cause granulopenia, gastrointestinal bleeding, dyspnea, liver and kidney damage, and mental depression.[6] Therefore, the removal of naproxen from wastewater is crucial.

The methods used for removing naproxen from water are adsorption,[6] photo-transformation,[7] catalytic degradation,[8] electrochemical degradation[9] and biodegradation.[10] Adsorption as an efficient method has been widely researched in recent years due to the advantages of low costs and convenience.[11,12] Various adsorption materials used for pharmaceutical adsorption from aqueous solution include multi-walled carbon nanotubes,[13] activated carbon,[14] microcrystalline cellulose,[15] graphene/graphene oxide,[16] and metal–organic framework[17] *etc.* In addition, a significant group of adsorbents for pharmaceutical adsorption are natural clays due to their wide range of sources and low price.

Halloysite nanotubes (HNT) are tubular aluminosilicate clays with large specific surface area, nanotube structure, and good biocompatibility.[18,19] At the same time, due to the differences in the chemical composition of the inner and outer surfaces of HNT (the outer surface is composed of Si–O, and the surface of the inner cavity is composed of Al–OH) and the charge properties (the inner surface is positively charged, and the outer surface is negatively charged), it can be used in fields such as adsorption,[20] oil water separation,[21] catalysis,[22] and drug release.[23] Their application is limited due to poor native adsorption properties. In order to improve the adsorption performance of HNT, various treatment methods including organic modification, intercalation modification, free radical modification, and surfactant modification can be used.[24] Dopamine modified HNT was used to remove U(VI) and the

[a]*College of Chemistry and Life Science, Sichuan Provincial Key Laboratory for Structural Optimization and Application of Functional Molecules, Chengdu Normal University, Chengdu, 611130, China. E-mail: zhonghli@sohu.com; guoweideng86@163.com*

[b]*Sichuan Key Laboratory of Medical Imaging & Department of Chemistry, School of Preclinical Medicine, North Sichuan Medical College, Nanchong, 637000, China*

adsorption performance was 72.51 mg g^{-1}.[25] Silane-modified halloysite/Fe_3O_4 nanocomposites were used for simultaneous removal of Cr(VI) and Sb(V).[26] A novel adsorbent was synthesized by immobilizing graphene oxide with halloysite nanotubes and used for the adsorption of levofloxacin and ciprofloxacin in a wide pH range.[27]

The purpose of this work was to synthesize a high-efficiency adsorbent for naproxen. Therefore, hybrid materials were synthesized using HNT as substrates by modifying polyaniline on their surfaces. The adsorbent was characterized using physicochemical methods and the effects of adsorption conditions were systematically researched. In addition, effects of ionic strength and metal ions, the adsorption kinetics, adsorption isotherm and mechanism for naproxen adsorption were also studied. This study promises to provide a new material for the efficient adsorption of naproxen and expand the application of halloysite nanotubes in the field of pharmaceutical wastewater treatment.

Experimental

Materials

All chemicals are analytical grade. Halloysite nanotubes was purchased from Xi'an Ming-chuang-da Biotechnology Co., Ltd. Aniline, ammonium persulfate and naproxen were obtained from Adamas (Shanghai, China). HCl, NaCl, NaOH, and ethanol were obtained from Chengdu Kelong Chemical Reagent Factory (Chengdu, China). Metal ion standard solution of Al^{3+}, Pb^{2+}, Cu^{2+}, Zn^{2+}, Co^{2+} and Fe^{3+} was purchased from Guobiao (Beijing) Testing & Certification Co., Ltd. (1 mg mL^{-1} in 1 M HNO_3).

Characterization

Scanning electron microscope (SEM, ZEISS Merlin), transmission electron microscope (TEM) and energy dispersive analysis of X-rays (EDS) of FEI Talos F200S from Thermo Fisher were used for observing the morphology of the HNT and HNT@PA-2. In addition, the specific surface area (BET), pore size and pore volume of HNT@PA-2 were determined by a pore size analyzer (ASAP 2020 V4.03, Micromeritics, USA). The crystal structure of HNT, HNT@PA-2, HNT@PA-1 and HNT@PA-0.5 was obtained by Powder X-ray diffraction (XRD) from Bruker D8 of Germany with a Cu Kα radiation in the 2θ range of 10–80°. Functional group structure information of HNT, HNT@PA-2, HNT@PA-1 and HNT@PA-0.5 was recorded by Fourier transform infrared spectrometer (FT-IR, Nicolet iS50, Thermo Scientific, USA). X-ray photo-electron spectrometer (XPS, K-Alpha) was used for collecting XPS spectrum of HNT and HNT@PA-2 by Thermo Scientific. The absorbance before and after adsorption was obtained by UV-2600 ultraviolet absorption spectrometer of Shimadzu (Suzhou).

Preparation of polyaniline-modified halloysite nanotubes

Halloysite nanotubes (0.75 g) were dispersed into 50 mL of distilled water by ultrasonic. The solution including aniline (1.5 mL) and 1 mol L^{-1} HCl (135 mL) were added into the dispersion of HNT by stirring at 10 °C. Initiator agent of ammonium persulfate (3.75 g, APS) was dissolved in 150 mL of 1 mol L^{-1} HCl mixture and added to the polymerization reaction system gradually within 90 minutes. The polymerization took place at room temperature for 4 h. The halloysite nanotubes modified by polyaniline (HNT@PA) was filtered and washed with distilled water to neutral. Finally, the product (HNT@PA-2) was dried in a vacuum oven at 70 °C for 48 hours. In addition, the product of the ratio of HNT to aniline as 1 : 1 (HNT@PA-1) and 1 : 0.5 (HNT@PA-0.5) were synthesized as the same method. The synthesis method of HNT@PA was shown in Fig. 1.

Adsorption experiments

The stock solution of naproxen (50 mg mL^{-1}) was prepared by dissolving naproxen in ethanol. The working solution of naproxen was prepared by diluting stock solution with distilled water. In order to evaluate the effect of adsorbent type on naproxen adsorption, 20 mg of HNT@PA-2, HNT@PA-1 and HNT@PA-0.5 were respectively placed in 20 mL of 20 μg mL^{-1} naproxen solutions at pH ranged from 3 to 10. The pH of naproxen adsorption was adjusted by 0.1 mol L^{-1} HCl and 0.1 mol L^{-1} NaOH. Then, the mixture was shaken at room temperature for 4 h. Other experimental conditions, such as the dosage of HNT@PA-2, initial concentration of naproxen, adsorption time and temperature were systematically investigated as the adsorption procedure as above. Different dosage of HNT@PA-2 (5, 10, 15, 20, 25 mg) was added in 20 mL of 20 μg mL^{-1} naproxen solutions at pH 9 and was shaken at room temperature for 4 h. In order to discuss the adsorption time for naproxen adsorption, 10 mg of HNT@PA-2 was added in 20 mL of 20 μg mL^{-1} naproxen solutions at pH 9 and was shaken at room temperature with different time (10, 20, 30, 40, 60, 120, 240, 480, 780 min). The initial concentration at different temperatures has different effects on the adsorption of naproxen. Therefore, 10 mg of HNT@PA-2 was added in 20 mL of different initial concentration of naproxen solutions (15, 20, 25, 30, 35, 40 μg mL^{-1}) at pH 9 and was shaken at 25, 35, 45 °C for 4 h.

Effect of ionic strength and metal ions

In order to evaluate the effect of ionic strength and metal ions on the adsorption of for naproxen by HNT@PA-2, 20 mg of HNT@PA-2 with 20 mL of 20 mg L^{-1} naproxen solutions under different NaCl concentrations (0.05, 0.1, 0.2, 0.3, 0.4, 0.5 mol L^{-1}) and different metal ions concentrations (0.01, 0.1, 1, 5, 10 μg mL^{-1}) were shaken at 20 °C for 4 h. The types of metal ions include Al^{3+}, Pb^{2+}, Cu^{2+}, Zn^{2+}, Co^{2+} and Fe^{3+}.

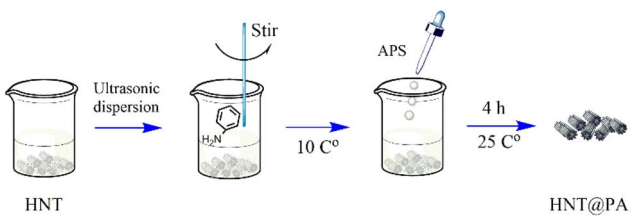

Fig. 1 The synthesis method of HNT@PA.

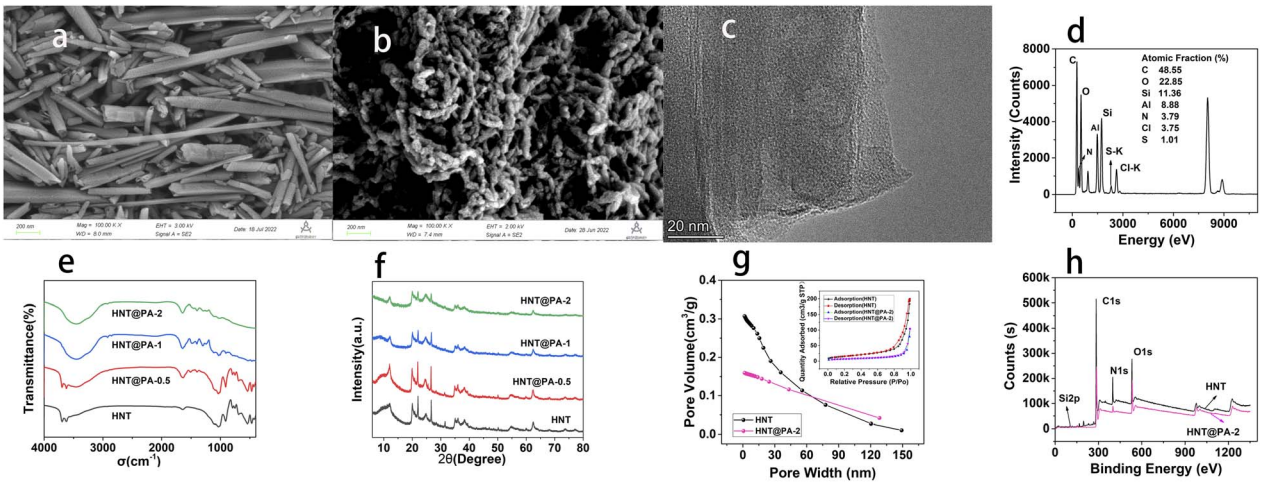

Fig. 2 The SEM images of HNT (a) and HNT@PA-2 (b). The TEM image (c) and EDS analysis (d) of HNT@PA-2. (e) The FTIR spectra of HNT, HNT@PA-2, HNT@PA-1 and HNT@PA-0.5. (f) The XRD curve of HNT, HNT@PA-2, HNT@PA-1 and HNT@PA-0.5. (g) The pore volume of HNT and HNT@PA-2. (h) XPS spectra of HNT and HNT@PA-2.

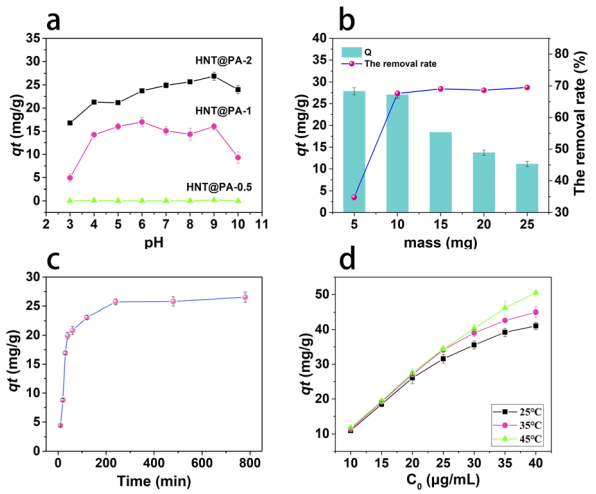

Fig. 3 Adsorption conditions of naproxen ((a) pH. (b) mass of HNT@PA-2. (c) time. (d) initial concentration of naproxen at 25, 35 and 45 °C).

Data analysis

After adsorption, the mixture was centrifuged for 5 minutes at 7000 rpm, and the absorbance of the supernatant was measured at 360 nm by ultraviolet spectrophotometer. The calibration curve of naproxen was $y = 0.01717x + 0.03833$ ($R^2 = 0.99973$).

The removal rate ($\eta\%$) and adsorption capacity (q) were evaluated by eqn (1) and (2):

$$\eta\% = \frac{c_0 - c_t}{c_0} \times 100\% \quad (1)$$

$$q = \frac{(c_0 - c_t)}{m} \times 100\% \quad (2)$$

where c_0 (μg mL^{-1}) is the initial concentration of naproxen, c_t (μg mL^{-1}) is the concentration of naproxen at time of t. m (mg) is the dosage of HNT@PA-2, and V (mL) is the volume of naproxen solution.

Results and discussion

Characterization of adsorbent

The SEM images of HNT and HNT@PA-2 were showed in Fig. 2(a) and (b). As can be seen from Fig. 2(a), the halloysite nanotubes were hollow tubular structure. When it was modified by polyaniline, the surface of the HNT becomes unsmooth with polymer formation. SEM images indicated that polyaniline had been successfully grown on the surface of HNT. TEM image (Fig. 2(c)) showed the surface of HNT@PA-2 become rougher, also illustrated that polyaniline was successfully modified on the surface of HNT. EDS analysis of HNT@PA-2 was shown in Fig. 2(d). The elements of C, O, Si, Al, N, Cl and S were detected in HNT@PA-2 with the atomic fraction at 48.55, 22.85, 11.36, 8.88, 3.79, 3.75 and 1.01%. The FTIR spectra of HNT, HNT@PA-0.5, HNT@PA-1 and HNT@PA-2 were shown in Fig. 2(e). With the increase of the amount of aniline, some new peaks appeared on the infrared spectrum. The –N–H stretching vibration band was at 3461.6 cm^{-1}. 1645.0 cm^{-1} and 1457.9 cm^{-1} was C=C stretching vibration of benzenoid ring. The band of 1108.8 cm^{-1} and 1230.3 cm^{-1} was =N$^+$-stretching vibration of quinonoid unit and C–N$^+$ stretching vibration of benzenoid unit, respectively.[28] These bands were polyaniline characteristic bands. These results illustrated that polyaniline was successfully

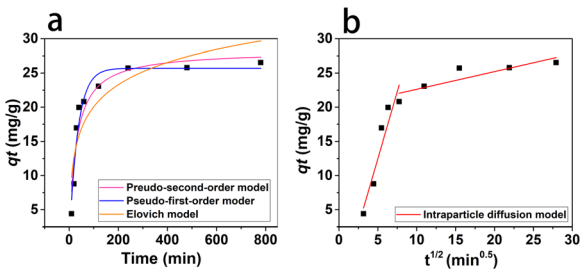

Fig. 4 The non-linear fitting curve of PFO, PSO and Elovich model (a) and linear fitting curve of intraparticle diffusion model (b).

Table 1 Fitting results of adsorption kinetic model

Model	Parameter	Value (μg mL^{-1})
Pseudo-first-order	q_t (mg g^{-1})	25.70
	k_1 (min^{-1})	0.03
	R^2	0.94
Pseudo-second-order	q_t (mg g^{-1})	28.27
	k_2 (g (mg^{-1} min^{-1}))	0.001
	R^2	0.91
Elovich	α	3.25
	β	0.21
	R^2	0.78
Intra-particle diffusion	k_1 (mg (g^{-1} min$^{-1/2}$))	3.93
	R^2	0.87
	k_2 (mg (g^{-1} min$^{-1/2}$))	0.26
	R^2	0.71

modified on HNT. As shown in Fig. 2(f), the crystal faces of HNT, such as (100), (002), (110), (003), (210) at 20.1°, 24.8°, 35.1°, 38.4°, 54.8° were preserved.[27] The XRD curves of HNT@PA-2, HNT@PA-1 and HNT@PA-0.5 were simisly as HNT illustrated that the modification of polyaniline did not change the crystal structure of halloysite nanotubes. The pore volume and specific surface area of HNT and HNT@PA-2 were showed in Fig. 2(g). The BET Surface Area and pore volume of HNT was 56.4620 m^2 g^{-1} and 0.308597 cm^3 g^{-1}. Compared with HNT, the BET Surface Area (24.2267 m^2 g^{-1}) and pore volume (0.161032 cm^3 g^{-1}) of HNT@PA-2 both decrease. The results showed that the polymerization of aniline on the surface of halloysite nanotubes reduced the specific surface area and pore volume. As shown in Fig. 2(h), it is obvious mainly consists of C, N, O and Si of HNT. In addition, the binding energies of C 1s, O 1s, N 1s and Si 2p was located at 284.04, 531.68, 398.67, and 102.06 eV, respectively in XPS spectra of HNT@PA-2. The high-resolution spectra of C 1s, O 1s, N 1s were shown and discussed detail in the part of Adsorption mechanisms.

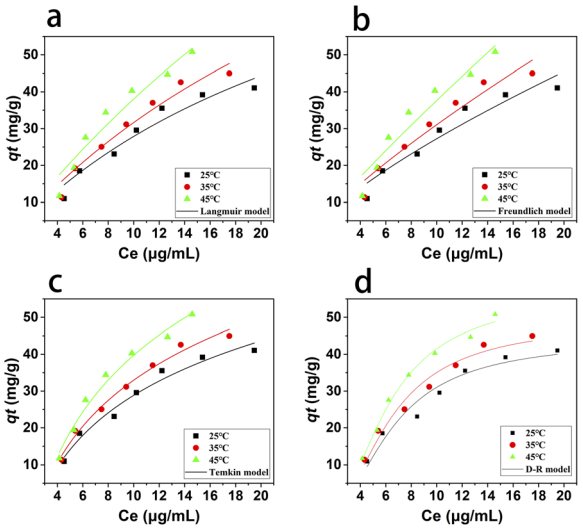

Fig. 5 The non-fitting result of adsorption isotherm for Langmuir model (a), Freundlich model (b), Temkin model (c) and D-R model (d).

Adsorption experiments

The effect of experimental conditions. The pH affects the form of naproxen in solution, resulting great influence on its adsorption. Therefore, the adsorption of naproxen under different pH was discussed firstly. There kinds of HNT@PA including HNT@PA-2, HNT@PA-1 and HNT@PA-0.5 were used. As shown in Fig. 2a, the adsorption capacity of HNT@PA-2 was the largest and the adsorption of naproxen on HNT@PA-0.5 was almost negligible. The results showed that the adsorption of naproxen increased with the increase of polyaniline content on halloysite nanotubes. The modification of polyaniline on halloysite nanotubes increases the adsorption of naproxen. Due to the introduction of polyaniline on HNT, active adsorption sites increased. The reason maybe that the diaromatic rings on naproxen and the benzene ring on polyaniline may be combined due to π–π interaction.[6] For pH ranged from 3 to 10, the adsorption capacity was highest at pH 9. The point of zero charge (pH_{PZC}) of HNT@PA-2 was estimated according to the pH drift method and the value was 3.4. When pH of solution above 3.4, the HNT@PA-2 was negatively charged. On the contrary, the HNT@PA-2 was positively charged. The pK_a for naproxen is 4.6. At pH 9, the HNT@PA-2 with negatively charged and naproxen with negatively charged, these illustrated that electrostatic adsorption is not the reason for naproxen adsorption on HNT@PA-2. Therefore, pH of 9 was selected as the optimum pH for naproxen adsorption.

Table 2 Adsorption isotherm model

Model	Parameter	Temperature (K) 298	308	318
Langmuir	q_m (mg g^{-1})	108.36	145.88	242.58
	K_L (L mg^{-1})	0.04	0.03	0.02
	R^2	0.94	0.95	0.93
Freundlich	K_F (mg g^{-1})	4.97	4.94	4.96
	n	1.35	1.25	1.13
	R^2	0.92	0.94	0.92
Temkin	K_T (J mol^{-1})	21.35	24.59	30.17
	f (L mg^{-1})	0.39	0.38	0.37
	R^2	0.97	0.99	0.98
D-R	q_m (mg g^{-1})	44.04	48.83	56.82
	R^2	0.95	0.97	0.99

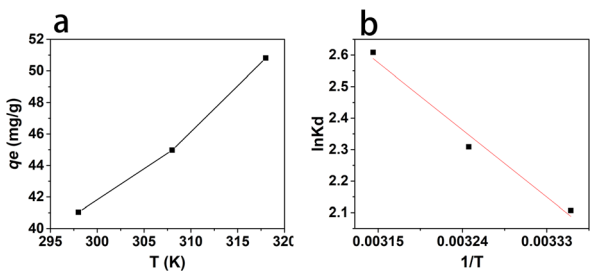

Fig. 6 Naproxen adsorption onto HNT@PA-2 at 298, 308 and 318 K (a) and the relationship between 1/T and ln K_d (b).

Table 3 Parameters of thermodynamic for the adsorption of naproxen

	T (K)	ΔG (kJ mol^{-1})	ΔH (kJ mol^{-1})	ΔS (J mol^{-1} K^{-1})
Naproxen	298	−1.85	2.37	10.04
	308	−2.14		
	318	−2.53		

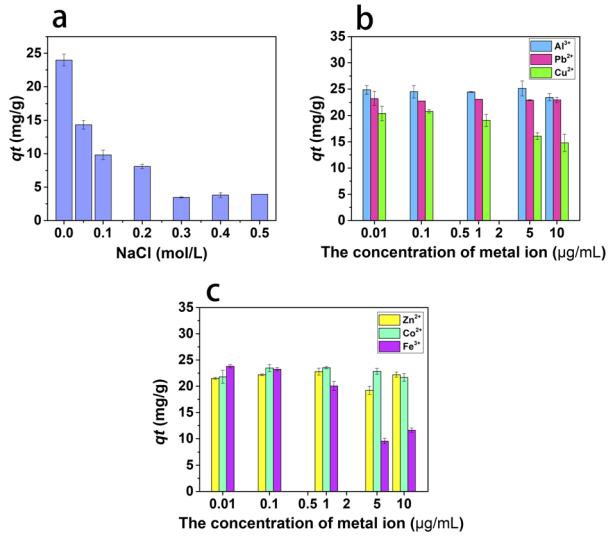

Fig. 7 Effect of ionic strength (a) and metal ions (b and c).

As shown in Fig. 3b, when the mass of HNT@PA-2 increase, the adsorption capacity of naproxen decreased. The removal rate of naproxen increased and finally stabilized at 70%. The reason for this result may be that more active adsorption sites are provided with the increase of mass of HNT@PA-2 resulting in the increase of removal rate. When the mass is greater than 10 mg, the removal rate tends to be stable. Therefore, 10 mg was selected as the best adsorbent mass.

The contact time is another important factor affecting adsorption. As shown in Fig. 3c, with the increase of contact time, the adsorption capacity of naproxen increased and reached adsorption equilibrium in 240 min. It may be that the adsorption active site has been occupied by naproxen, and the adsorption capacity will not be increased by increasing the contact time. Therefore, 4 h was selected as the best contact time.

The result of influence on adsorption with the initial concentration of naproxen solutions at 25, 35 and 45 °C was shown in Fig. 3d. With the increase of initial concentration, the adsorption capacity of naproxen increased. With the increase of temperature, the adsorption capacity also increased. The results showed that the increasing of initial concentration provided more naproxen molecules that can be adsorbed in the HNT@PA-2 which resulting in the increase of adsorption capacity. High temperature was favourable for adsorption, which indicated that the adsorption of naproxen on HNT@PA-2 was endothermic. The reason may be that the migration rate of naproxen molecules from aqueous solution to HNT@PA-2 increases under high temperature.

Adsorption kinetics. In this work, pseudo-first-order model (PFO, eqn (3)), pseudo-second-order model (PSO, eqn (4)) and Elovich model (eqn (5)), and intraparticle diffusion model (eqn (6)) were applied to describe the adsorption of naproxen onto HNT@PA-2.

$$q_t = q_e(1 - e^{-k_1 t}) \quad (3)$$

$$q_t = \frac{k_2 q_e^2 t}{1 + k_2 q_e t} \quad (4)$$

$$q_t = \frac{1}{\beta}\ln(1 + \alpha\beta t) \quad (5)$$

$$q_t = k_p t^{0.5} + C \quad (6)$$

where q_t (mg g^{-1}) is the adsorption capacity at time t; q_e (mg g^{-1}) is the equilibrium adsorption capacity; k_1 (min^{-1}), k_2 (g (mg^{-1} min^{-1})), β (g mg^{-1}) and k_p (mg (g^{-1} min$^{-0.5}$)) is the rate constant of PFO, PSO model, Elovich model and intraparticle diffusion model, respectively; α (mg (g^{-1} min^{-1})) is initial adsorption rate in Elovich model.

The non-linear fitting curve of PFO, PSO and Elovich model for naproxen adsorption on HNT@PA-2 was shown in Fig. 4a. The linear fitting curve of intraparticle diffusion model was shown in Fig. 4b. Detailed fitting results were listed in Table 1. Compared with other kinetics model, the correlation coefficient (R^2) calculated from the PFO model was the highest (0.94). Additionally, the experimental value of adsorption capacity (26.07 mg g^{-1}) was consistent with the q_e value obtained from the PFO mode (25.70 mg g^{-1}). These results illustrated that the adsorption of naproxen on HNT@PA-2 conformed to PFO kinetic model. In the PFO kinetic model, the transport of adsorbate from solution to the adsorbent surface was controlled by diffusion steps. The results showed that naproxen adsorbed to HNT@PA-2 surface was mainly based on physical adsorption.[29]

Adsorption isotherms. The adsorption isotherm is the relationship curve between the concentration of solute molecules in the liquid and solid two-phases when the adsorption process on the two-phase interface reaches equilibrium. The Langmuir (eqn (7)), Freundlich (eqn (8)), Temkin (eqn (9)) and D-R (eqn (10)) models were applied to fit the adsorption isotherm process.

$$q_e = \frac{q_m k_L c_e}{1 + k_L c_e} \quad (7)$$

$$q_e = k_F c_e^{1/n} \quad (8)$$

$$q_e = k_T \ln(f c_e) \quad (9)$$

$$q_e = q_m \exp(-\beta\varepsilon^2) \quad (10)$$

where q_m (mg g^{-1}) is the maximum adsorption capacity; q_e (mg g^{-1}) is the equilibrium adsorption capacity; c_e (μg mL^{-1}) is the equilibrium concentration of naproxen after adsorption; k_L (L mg^{-1}), k_F (mg g^{-1}), and k_T (J mol^{-1}) is the Langmuir constant, Freundlich constant and Temkin constant, respectively; n is adsorption intensity in Freundlich model; ε is D-R isotherm constant and β (mol^2 kJ^{-2}) is a constant in related to the mean free energy of adsorption in D-R model; f (L mg^{-1}) is Temkin isotherm equilibrium binding constant.

The non-linear fitting curves of the isothermal adsorption for naproxen on HNT@PA-2 were shown in Fig. 5 and its fitting parameters were shown in Table 2. With the increase of temperature, at the same initial concentration of naproxen, the equilibrium concentration decreased and the adsorption capacity increased. The results illustrated that endothermic will promote the adsorption of naproxen onto HNT@PA-2.

At the three experimental temperatures, the fitting correlation coefficient (R^2) of Langmuir model was higher than Freundlich model, indicating that naproxen was uniformly adsorbed on the HNT@PA-2 surface and there were a certain number of adsorption sites on the HNT@PA-2 surface. The energy of all adsorption sites was same. When the adsorption was balanced, the adsorption rate and desorption rate were equal. According to the fitting results of Langmuir model, the maximum adsorption capacity of HNT@PA-2 for naproxen was 242.58 mg g^{-1} at 318 K. Compare the value of R^2 fitted by each model, the Temkin model had the largest value of R^2. The Temkin model considers the effect of the interaction between adsorbent and adsorbate, and the adsorption heat of all molecules is linearly decreasing with the coverage. In addition, the fitting results of D-R model were also in good agreement, indicating that the adsorption of naproxen by HNT@PA-2 also included the adsorption behavior on the surface of microporous adsorbent.

Adsorption thermodynamics. Thermodynamic constants containing Gibbs free energy change (ΔG), enthalpy change (ΔH) and entropy change (ΔS) were determined by the following equation:

$$\Delta G = -RT \ln K_d \tag{11}$$

$$\Delta G = \Delta H - T\Delta S \tag{12}$$

$$\ln K_d = \frac{\Delta S}{R} - \frac{\Delta H}{RT} \tag{13}$$

$$K_d = \frac{q_e}{c_e} \tag{14}$$

where K_d is the equilibrium constant; R is the gas constant (8.314 J mol^{-1} K^{-1}); T is the absolute temperature (K); c_e (μg mL^{-1}) is the equilibrium concentration of naproxen; q_e is the equilibrium adsorption capacity (mg g^{-1}).

As shown in Fig. 6a, the adsorption capacity of HNT@PA-2 for naproxen increased with the increase of temperature. The relationship between $1/T$ and $\ln K_d$ was plotted in Fig. 6b. As shown in Table 3, the negative values of ΔG illustrated that the adsorption of naproxen on HNT@PA-2 was spontaneous. The value of ΔG was −1.85, −2.14, and −2.53 kJ mol^{-1} at 298, 308 and 318 K suggesting that the higher spontaneity occurred at higher temperatures. The value of ΔH was positive and small (2.37 kJ mol^{-1}) showed that the adsorption was endothermic process, and the physical binding plays an important role. At the same time, $\Delta S > 0$ indicated that the randomness of the system increases with the increase of temperature. Therefore, the adsorption of naproxen by HNT@PA-2 was endothermic and spontaneous.

Effect of ionic strength and metal ions. The ion strength has a great influence on the adsorption by the electrostatic and nonelectrostatic interactions between adsorbent and adsorbate. NaCl is the most common ion in the environment. Therefore,

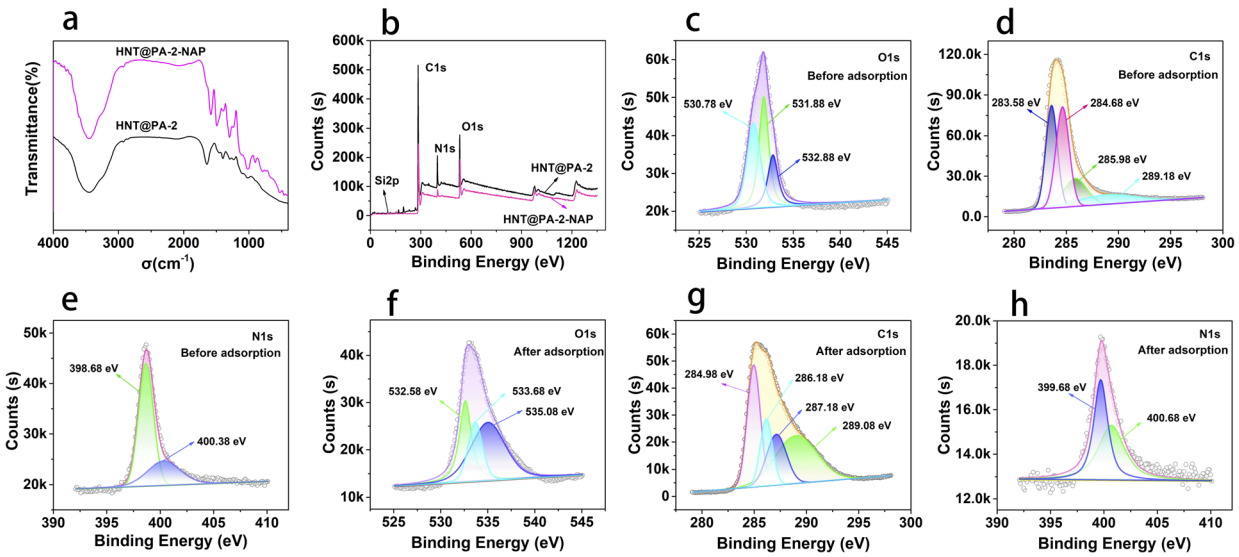

Fig. 8 The FT-IR spectrum (a) and XPS spectrum (b) of HNT@PA-2 and HNT@PA-2-NAP. The XPS high resolution spectra of O 1s, C 1s and N 1s before adsorption (c–e) and after adsorption (f–h).

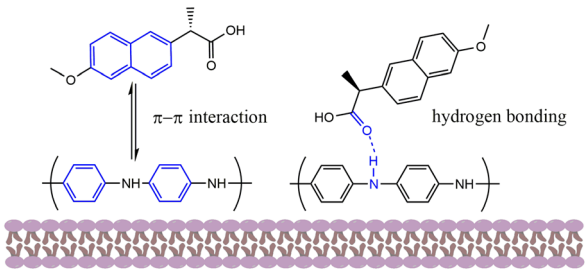

Fig. 9 The possible adsorption mechanisms of naproxen on HNT@PA-2.

NaCl is selected to study the adsorption of ion strength on naproxen. As shown in Fig. 7a, the adsorption capacity of naproxen on HNT@PA-2 decreases with the increase of NaCl concentration. When the concentration of NaCl was above 0.3 mol L^{-1}, the adsorption tended to be stable. In general, the outer sphere adsorption was easily affected by the ionic strength, while the inner sphere adsorption was opposite.[30] When the NaCl concentration was <0.3 mol L^{-1}, the outer sphere adsorption was dominant. When the NaCl concentration was between 0.3 and 0.5 mol L^{-1}, the inner sphere adsorption was dominant. Hence, the adsorption of naproxen on HNT@PA-2 involved both outer sphere adsorption and inner sphere adsorption.

Heavy metal ions and drugs will coexist in the environment, which may cause complex pollution. Therefore, the metal ions such as Al^{3+}, Pb^{2+}, Cu^{2+}, Zn^{2+}, Co^{2+} and Fe^{3+} had been used to study the effect of metal ion of naproxen adsorption on HNT@PA-2. As shown in Fig. 7b and c, the adsorption capacities had no significant change as the Al^{3+}, Pb^{2+}, Zn^{2+} and Co^{2+} ion concentrations increased from 0.01 to 10 μg mL^{-1}. However, the adsorption capacities of naproxen decreasing with the increasing concentrations of Cu^{2+} and Fe^{3+} ions added into the system. Based on this phenomenon, the presence of Cu^{2+} and Fe^{3+} ions inhibited the adsorption of naproxen on HNT@PA-2, while Al^{3+}, Pb^{2+}, Zn^{2+} and Co^{2+} ions had negligible effects on its adsorption. Possible reasons for inhibiting adsorption of Cu^{2+} and Fe^{3+} ions were that HNT@PA-2 has better adsorption capacity for metal ions, and most of the active adsorption sites of HNT@PA-2 were occupied by Cu^{2+} and Fe^{3+} ions, therefore the adsorption was inhibited. In addition, the electrostatic interaction between Cu^{2+} and Fe^{3+} ions and HNT@PA-2 might another reason for adsorption on HNT@PA-2.

Adsorption mechanisms. FT-IR and XPS were used to analyse the changes of the adsorbent before and after adsorption. As shown in Fig. 8a, the shapes of FT-IR spectrum for HNT@PA-2 before and after adsorption were similar, but some new peaks appeared after adsorption. The main new absorption bands occurred at 1583.6, 1493.3, 1296.3, and 903.2 cm^{-1}. The band at 1493.3 cm^{-1} was attributed to C=C stretching vibration in benzene ring. The band at 1296.3 cm^{-1} due to C–O stretching vibration of naproxen.[31] The characteristic peaks of benzene ring were obviously stronger which is powerful evident for the adsorption of naproxen onto HNT@PA-2. In addition, the peak at 1645.0 cm^{-1} of HNT@PA-2 attributable to the stretching vibrations of C=O groups shifted to a lower frequency after adsorption (1583.6 cm^{-1}), indicating that the carbonyl groups were participating in hydrogen bonding.

The survey scan spectrum of HNT@PA-2 before and after adsorption were listed in Fig. 8b, including C1s, O1s, N1s, and Si2p. As shown in Fig. 8c, the high resolution O 1s spectrum of HNT@PA-2 was divided into three peaks were located at 530.78, 531.88 and 532.88 eV which were attributed to O–H, C=O and C–O–C, respectively. After naproxen adsorption, the high resolution O 1s spectrum had a small shift to 532.58, 533.68 and 535.08 eV (Fig. 8f). The four high resolution spectra's of C 1s as 283.58, 284.68, 285.98 and 289.18 eV, which could be attributed to C=C, C–N, C–O–C and C=O (Fig. 8d). After naproxen adsorption, the binding energy of C=C (284.98 eV), C–N (286.18 eV), C–O–C (287.18 eV) and C=O (289.08 eV) also had a small shift compared with HNT@PA-2 (Fig. 8g). In addition, as shown in Fig. 8e and h, the binding energy of 398.68 and 400.38 eV were assigned to C–N. The binding energy of N1s were negligible changes before and after adsorption. These results indicated that oxygen and carbon-containing functional groups were involved in the adsorption of naproxen. This was confirmed by elemental analysis compositions of HNT@PA-2 were obtained by EDS analysis with the higher atomic fraction at 48.55% (C) and 22.85% (O). HNT@PA-2 with benzene ring could bind with diaromatic rings of naproxen. The adsorbate may combine with the adsorbent through hydrogen bonding, π–π interaction, electrostatic interaction as well as hydrophobic reaction. Through pH analysis, electrostatic interaction was excluded. Therefore, naproxen was adsorbed on HNT@PA-2 might because of π–π interaction, hydrogen bonding and hydrophobic reaction. The possible adsorption mechanisms of naproxen on HNT@PA-2 were presented in Fig. 9.

Table 4 Comparison of adsorption capacity for several adsorbents

Adsorbents	Order of adsorption	q_m (mg g^{-1})	Ref.
Al-MOF-Fe_3O_4@P4VP	PSO	226.24	6
PAMAM-halloysite hybrid	PSO	8.08	32
Gel-1.0MOF-Sep	PSO	8.515	33
Cu-doped Mil-101(Fe)	PSO	396.5	34
Activated carbons	PSO	3.23	35
Magnetic iron/copper nanoparticles	PFO	—	36
HNT@PA-2	PFO	242.58	This work

Comparison of various adsorbents. The comparison of adsorption capacities of naproxen by several adsorbents were listed in Table 4. The adsorption capacity of naproxen on HNT@PA-2 is not the largest, but halloysite nanotube have a wide range of sources, inexpensive, and easily to modify. In addition, the synthetic method of is HNT@PA-2 is simple. Therefore, HNT@PA-2 have great potential for use as a naproxen adsorbent.

Conclusions

Polyaniline modified halloysite nanotubes were used for the adsorption of naproxen was prepared by *in situ* polymerization. Polyaniline was introduced to halloysite nanotubes to increase active adsorption sites. The optimal ratio of halloysite nanotubes to aniline was 1 : 2. The adsorption of naproxen conformed to PFO kinetic model, and the maximum adsorption capacity was 242.58 mg g^{-1} at 318 K. The mechanisms for naproxen adsorbed by the HNT@PA-2 were π–π interaction and hydrophobic reaction. Al^{3+}, Pb^{2+}, Zn^{2+} and Co^{2+} ions had negligible effects on naproxen adsorption, and Cu^{2+} and Fe^{3+} ions inhibited adsorption. Therefore, the polyaniline modified halloysite nanotubes are promising naproxen adsorbents that could be used for the treatment of medical wastewater.

Author contributions

Qihui Wang: data curation, methodology, investigation, writing – original draft. Minghui Huang, Ying Zhu: data curation. Jiexue Wang, Zihang He, Jun Liu: writing – review. Kang Sun: writing – review & editing. Zhonghui Li, Guowei Deng: funding acquisition, project administration.

Conflicts of interest

There are no conflicts to declare.

Acknowledgements

This work was supported by the project of Chengdu Normal University (No. CS18ZDZ01, No. CS19ZA04), the Sichuan Provincial Students' Innovation and Entrepreneurship Training Program (No. S202214389159), the Opening Project of Medical Imaging Key Laboratory of Sichuan Province (No. MIKL202203), the Scientific Research Innovation Team Funds of Chengdu Normal University (No. CSCXTD2020A05).

References

1 S. Wöhrl, *Allergo J. Int.*, 2018, **27**, 114–121.
2 D. N. Bateman, *Medicine*, 2012, **40**, 140.
3 M. Afzali, Z. Jahromi and R. Nekooie, *Microchem. J.*, 2019, **145**, 373–379.
4 W. Sun, H. Li, H. Li, S. Li and X. Cao, *Chem. Eng. J.*, 2019, **360**, 645–653.
5 O. Paunovic, S. Pap, S. Maletic, M. A. Taggart, N. Boskovic and M. Turk Sekulic, *J. Colloid Interface Sci.*, 2019, **547**, 350–360.
6 Y. Li, Y. Wang, L. He, L. Meng, H. Lu and X. Li, *J. Hazard. Mater.*, 2020, **383**, 121144.
7 D. Górny, U. Guzik, K. Hupert-Kocurek and D. Wojcieszyńska, *Ecotoxicol. Environ. Saf.*, 2019, **167**, 505–512.
8 R. Bai, Y. Xiao, W. Yan, S. Wang, R. Ding, F. Yang, J. Li, X. Lu and F. Zhao, *Environ. Sci. Pollut. Res.*, 2020, **27**, 21542–21551.
9 L. Xu, X. Ma, J. Niu, J. Chen and C. Zhou, *J. Hazard. Mater.*, 2019, **379**, 120692.
10 T. Ding, K. Lin, B. Yang, M. Yang, J. Li, W. Li and J. Gan, *Bioresour. Technol.*, 2017, **238**, 164–173.
11 M. Hong, L. Yu, Y. Wang, J. Zhang, Z. Chen, L. Dong, Q. Zan and R. Li, *Chem. Eng. J.*, 2019, **359**, 363–372.
12 G. Zhang, Y. Liu, S. Zheng and Z. Hashisho, *J. Hazard. Mater.*, 2019, **364**, 317–324.
13 H. Zhao, X. Liu, Z. Cao, Y. Zhan, X. Shi, Y. Yang, J. Zhou and J. Xu, *J. Hazard. Mater.*, 2016, **310**, 235–245.
14 N. Magesh, A. A. Renita, R. Siva, N. Harirajan and A. Santhosh, *Chemosphere*, 2022, **290**, 133227.
15 B.-G. Cho, S.-B. Mun, C.-R. Lim, S. B. Kang, C.-W. Cho and Y.-S. Yun, *J. Hazard. Mater.*, 2022, **426**, 128087.
16 X. Wang, H. Zhang, Y. Wei, L. Bao, S. Liu, S. Yuan and S. Yuan, *Colloids Surf., A*, 2022, **644**, 128864.
17 S. Lin, Y. Zhao and Y.-S. Yun, *ACS Appl. Mater. Interfaces*, 2018, **10**, 28076–28085.
18 F. Cravero and G. Jock Churchman, *Clay Miner.*, 2016, **51**, 417–427.
19 G. J. Churchman, P. Pasbakhsh and S. Hillier, *Clay Miner.*, 2016, **51**, 303–308.
20 X. Wang, H. Guo, F. Wang, T. Tan, H. Wu and H. Zhang, *J. Radioanal. Nucl. Chem.*, 2020, **324**, 1151–1165.
21 Q. Song, H. Wang, S. Han, J. Wang, B. Zhang and Y. Zhang, *Prog. Org. Coat.*, 2020, **148**, 105839.
22 Y. H. Ahmad, A. T. Mohamed and S. Y. Al-Qaradawi, *Appl. Clay Sci.*, 2021, **201**, 105956.
23 C. Cheng, Y. Gao, W. Song, Q. Zhao, H. Zhang and H. Zhang, *Chem. Eng. J.*, 2020, **380**, 122474.
24 C. Cheng, W. Song, Q. Zhao and H. Zhang, *Nanotechnol. Rev.*, 2020, **9**, 323–344.
25 T. Ou, Y. Wu, W. Han, L. Kong, G. Song, D. Chen and M. Su, *J. Hazard. Mater.*, 2022, **424**, 127208.
26 K. Zhu, Y. Duan, F. Wang, P. Gao, H. Jia, C. Ma and C. Wang, *Chem. Eng. J.*, 2017, **311**, 236–246.
27 Q. Wang, M. Yang, X. Qi, J. Wang, K. Sun, Z. Li and G. Deng, *New J. Chem.*, 2021, **45**, 18315–18326.
28 Y. Zhao, Y. g. Li, X. Quan and C. Li, *Electrochim. Acta*, 2019, **321**, 134715.
29 M. N. Alnajrani and O. A. Alsager, *Sci. Rep.*, 2020, **10**, 794.
30 X. Ren, D. Shao, S. Yang, J. Hu, G. Sheng, X. Tan and X. Wang, *Chem. Eng. J.*, 2011, **170**, 170–177.
31 Y. Cao, A. Khan, A. Soltani, V. Erfani-Moghadam, A. N. K. Lup, M. Aghaei, N. Abdolahi, M. Khalili, M. Cordani, H. Balakheyli, S. Tavassoli and A. B. Albadarin, *Arabian J. Chem.*, 2021, **14**, 103190.

32 J. Kurczewska, M. Cegłowski and G. Schroeder, *Appl. Clay Sci.*, 2020, **190**, 105603.
33 L. K. Njaramba, M. Kim, Y. Yea, Y. Yoon and C. M. Park, *Chem. Eng. J.*, 2023, **452**, 139426.
34 P. Xiong, H. Zhang, G. Li, C. Liao and G. Jiang, *Sci. Total Environ.*, 2021, **797**, 149179.
35 R. L. T. Costa, R. A. do Nascimento, R. C. S. de Araújo, M. G. A. Vieira, M. G. C. da Silva, S. M. L. de Carvalho and L. J. G. de Faria, *J. Mol. Liq.*, 2021, **343**, 116980.
36 M. Şahin, Y. Arslan and F. Tomul, *Res. Chem. Intermed.*, 2022, **48**, 5209–5226.